Spring 2017

Characterization of the rectification behaviour of in-amps and estimating the near field coupling from SMPS circuits to a nearby antenna using dipole moments

Chunyu Wu

Department:

CHARACTERIZATION OF THE RECTIFICATION BEHAVIOUR OF IN-AMPS AND ESTIMATING THE NEAR FIELD COUPLING FROM SMPS CIRCUITS TO A NEARBY ANTENNA USING DIPOLE MOMENTS

by

CHUNYU WU

A THESIS

Presented to the Faculty of the Graduate School of the

MISSOURI UNIVERSITY OF SCIENCE AND TECHNOLOGY

In Partial Fulfillment of the Requirements for the Degree

MASTER OF SCIENCE IN ELECTRICAL ENGINEERING

2017

Approved by

Dr. Jun Fan, Advisor
Dr. David Pommerenke
Dr. Victor Khilkevich

ABSTRACT

This thesis discusses two parts.

In the first part, the rectification behavior of popular instrumentation amplifiers is measured in both common mode and single-ended RF noise injection. It is recommended that AD8221 be used in common mode RF noise injection environment. And AD8220 and AD8429 are recommended in single-ended RF noise injection environment. The mechanism of RF noise rectification inside in-amps is also discussed. It is verified that rectification mainly happens at the non-inverting input of two op-amps in the first stage of an in-amp. The DC voltage difference between inverting input and non-inverting input of the in-amp is further amplified, which will cause a large DC offset at the output. It is shown that symmetry of the first stage in an instrumentation amplifier is very important. The asymmetry of the first stage will increase the DC offset at the output dramatically. The layout of gain resistor should be symmetric to reduce DC offset at the output.

In the second part, the near field coupling from SMPS circuits to a nearby antenna is studied using dipole moments. The dipole moments are extracted from scanned H fields on a plane above SMPS circuits, and then imported into an HFSS model to do full wave simulation. The simulated coupling matches well with direct measurement. Methods to resolve magnitude and phase of near fields of SMPS noise source are also introduced.

ACKNOWLEDGMENTS

I would like to express my deep gratitude to my advisor, Dr. Jun Fan for his support and guide in professional skills, research method and working attitude, from which I have learned and benefitted a lot.

I also would like to express my thanks to Dr. David Pommerenke and Dr. Victor Khilkevich for their valuable advice and guide during my study.

I would also thank other faculty members and students in EMC Lab for their help in completing my master's degree.

Finally, I am deeply grateful to my parents and sisters for their love and encouragement.

TABLE OF CONTENTS

Page

ABSTRACT iii

ACKNOWLEDGMENTS iv

LIST OF ILLUSTRATIONS vi

LIST OF TABLES viii

SECTION

1. CHARACTERIZATION OF THE RECTIFICATION BEHAVIOUR OF IN-AMPS 1

1.1. INTRODUCTION 1

1.2. MEASUREMENT PREPARATION 3

1.2.1. Measurement Setup 3

1.2.2. Test Board Design 4

1.3. MEASUREMENT RESULTS 5

1.3.1. A Basic Look At Common Mode RF Noise Injection 5

1.3.2. Comparison Of Different IN-AMPS In Terms Of RF Noise Rectification 6

1.4. MECHANISM OF RF NOISE RECTIFICATION INSIDE IN-AMPS 9

1.5. WAYS TO REDUCE DC OFFSET AT THE OUTPUT 11

1.6. CONCLUSION 13

2. ESTIMATING THE NEAR FIELD COUPLING FROM SMPS CIRCUITS TO A NEARBY ANTENNA USING DIPOLE MOMENTS 15

2.1. INTRODUCTION 15

2.2. NEAR FIELD SCAN 17

2.2.1. How To Resolve Phase 17

2.2.2. How To Resolve Magnitude 21

2.3. DIPOLE-MOMENT MODEL EXTRACTION AND USAGE 22

2.4. COMPARISON OF SIMULATION AND DIRECT MEASUREMENT 24

2.5. CONCLUSION AND ERROR ANALYSIS 25

BIBLIOGRAPHY 27

VITA 28

LIST OF ILLUSTRATIONS

Page

Figure 1.1. The classic 3-op amp in-amp 1
Figure 1.2. Oscilloscope Image of Op Amp Output and Input 2
Figure 1.3. Measurement setup diagram 3
Figure 1.4. Schematic for DUT 4
Figure 1.5. DC Offset over frequency when gain is 1 5
Figure 1.6. DC Offset over frequency when gain is 10 5
Figure 1.7. Common mode RF noise injection 6
Figure 1.8. Single-ended RF noise injection 7
Figure 1.9. Comparison of different chips of AD8226 8
Figure 1.10. Comparison of single-ended RF noise injection 9
Figure 1.11. An in-amp built from three op-amps 10
Figure 1.12. Characterization of op-amp in terms of RF noise rectification 10
Figure 1.13. Comparison of direct measurement and calculated DC offset 11
Figure 1.14. Symmetry test 12
Figure 1.15. Effect of layout of gain resistor 13
Figure 2.1. The test board 16
Figure 2.2. Measured coupling from SMPS circuits to antenna with different RBW setting 16
Figure 2.3. Measurement setup to resolve phase using oscilloscope 17
Figure 2.4. Time domain waveform of field signal and reference signal 18
Figure 2.5. Time domain waveform in one period 19
Figure 2.6. Captured waveform during scan 20
Figure 2.7. Measurement setup to resolve phase using VNA 20
Figure 2.8. Scanned phase pattern of H field in x direction at 870MHz 21
Figure 2.9. Scanning setup for magnitude and scanned magnitude pattern of H field in x direction at 870MHz 22
Figure 2.10. Near field scan plane and dipole array plane[4] 22
Figure 2.11. An example text file describing the dipole information in HFSS 24

Figure 2.12. HFSS model with dipole moments imported 24
Figure 2.13. Comparison of simulation and direct measurement 25
Figure 2.14. S11 of antenna in simulation model and measurement 26

LIST OF TABLES

Page

Table 2.1. Comparison of simulation and direct measurement 25

1. CHARACTERIZATION OF THE RECTIFICATION BEHAVIOUR OF IN-AMPS

1.1. INTRODUCTION

An instrumentation amplifier is a type of differential amplifier that has been outfitted with input buffer amplifiers, which eliminate the need for input impedance matching and thus make the amplifier particularly suitable for use in measurement and test equipment. Additional characteristics include very low DC offset, low drift, low noise, very high open-loop gain, very high common-mode rejection ratio, and very high input impedances. Instrumentation amplifiers are used where great accuracy and stability of the circuit both short and long-term are required.

Although the instrumentation amplifier is usually shown schematically identical to a standard operational amplifier (op-amp), the electronic instrumentation amp is almost always internally composed of 3 op-amps. These are arranged so that there is one op-amp to buffer each input (+, −), and one to produce the desired output with adequate impedance matching for the function. The classic 3-op amp in-amp circuit is shown in Figure 1.1. It is composed of two stages: the first stage is called input section and the second stage is called output section. [1][2]

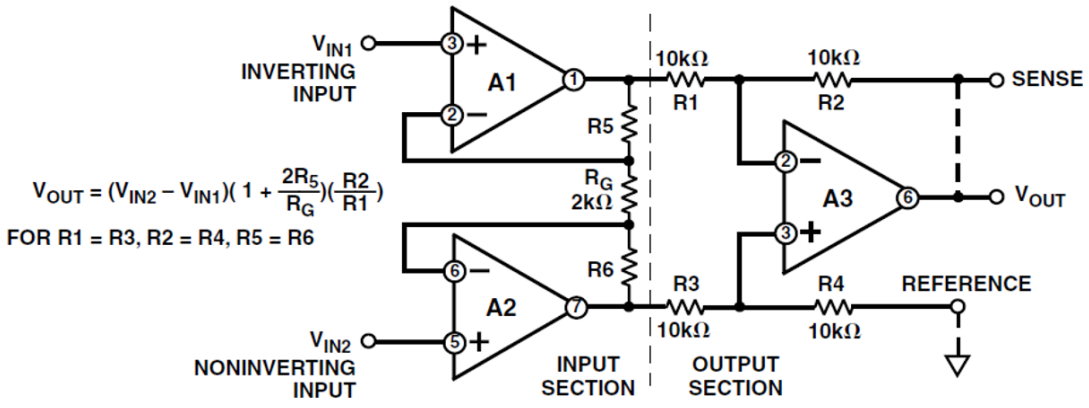

Figure 1.1. The classic 3-op amp in-amp

The most common op amp response to out-of-band EMI is a shift in the dc offset voltage that appears at the op amp output. Conversion of a high-frequency EMI signal to dc is the result of the nonlinear behavior of the internal diodes formed by silicon p-n junctions inside the device. This behavior is referred to as rectification because an ac signal is converted to dc. The small RF noise rectification generates a small dc voltage in the op amp circuitry. When this rectification occurs in the op amp signal path, the effect is amplified and may appear as a dc offset at the op amp output. Figure 1.2 shows an oscilloscope screenshot of an op amp output shift that occurs as an RF noise is applied to the op amp input. This effect is undesirable because it adds to the offset error. [3]

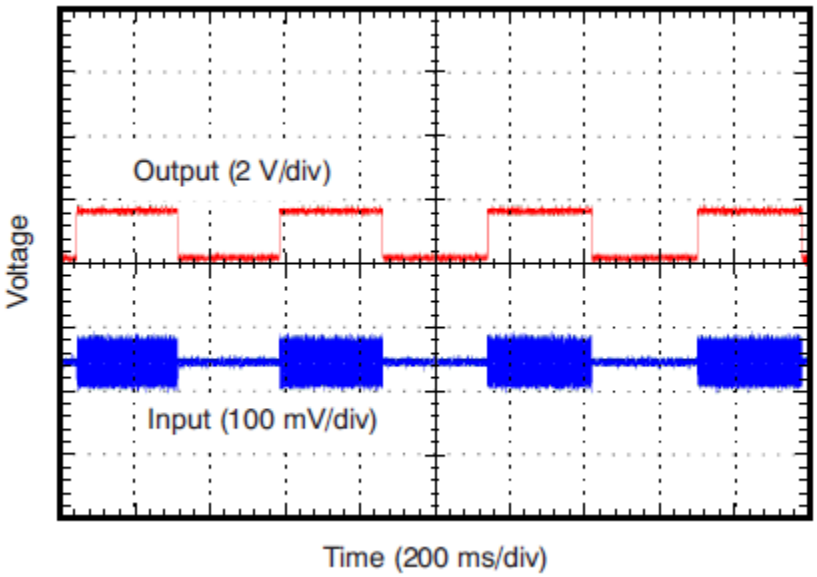

Figure 1.2. Oscilloscope Image of Op Amp Output and Input
(Gain = 100, GBW = 18 MHz, RF Input = 300-MHz CW)

In this thesis, the rectification behavior of popular instrumentation amplifiers is measured in both common mode and single-ended RF noise injection. The mechanism of RF noise rectification inside in-amps is studied. Possible ways that can help reduce the DC offset are also indicated.

1.2. MEASUREMENT PREPARATION

1.2.1. Measurement Setup. The diagram of measurement setup is shown in Figure 1.3. In this measurement setup, a RF generator is used to generate RF noise. Generated RF noise will be conducted to the test board using a cable. For the operation of in-amps, a DC power supply is used to provide ± 15V to in-amps. Another DC power supply is used to provide DC bias.

Oscilloscope is used to monitor the RF noise level at the input and measure the DC offset at the output of in-amps. The RF noise level at the input needs to be monitored because it is not consistent 50 ohm along the way from RF generator to in-amp pins, multiple reflections will occur, the RF noise level at the injected pins of the IC does not equal the forward RF noise level at the output of the RF generator. To measure the RF noise level, input impedance of the oscilloscope need to be configured to 50 Ohm to avoid reflections. All the instruments can be controlled by a computer to do automation measurement.

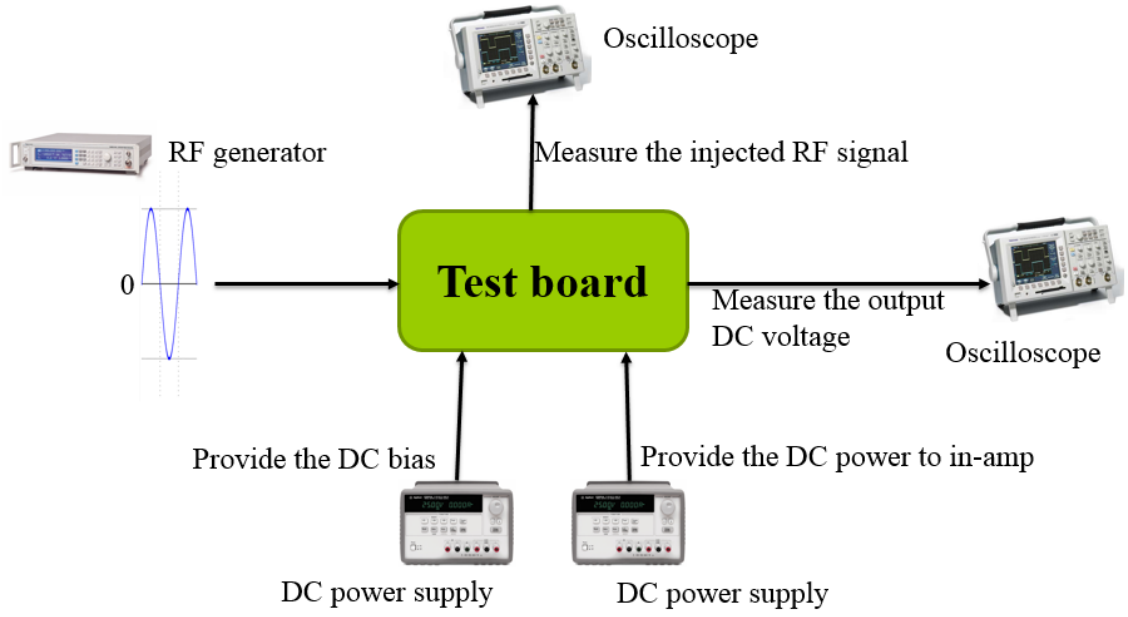

Figure 1.3. Measurement setup diagram

1.2.2. Test Board Design. The schematic of the test board is shown in Figure 1.4. Jumper J7 is used to configure the common mode RF noise injection and single-ended RF noise injection. Two DC blocks C8 and C9 are used to block DC voltage to avoid its influence on the RF generator. Two DC blocks C17 and C18 are used to make DC bias at IN+ and IN- equal DC power supply output voltage. 500 ohm resistor R9, R12 and R13 are used to reduce possible resonance. R11 and R14 will not be populated in common mode RF noise injection. In single-ended RF noise injection, R11 or R14 will be populated with a 0 ohm resistor.

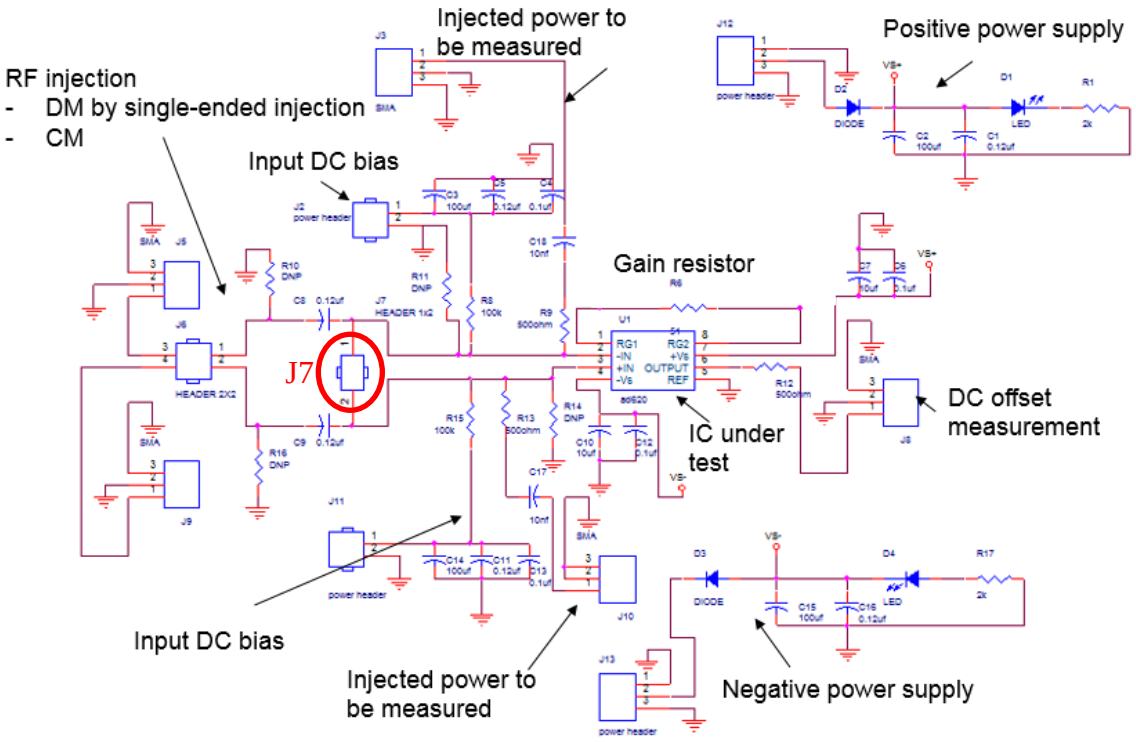

Figure 1.4. Schematic for DUT

1.3. MEASUREMENT RESULTS

1.3.1. A Basic Look At Common Mode RF Noise Injection. DC bias of IN+ and IN- is set to 1V. The power of injected RF noise is swept from -30dBm to 4dBm. -110dBm RF noise injection is used to observe the curve without RF noise injection as a reference. The gain of in-amp can be configured as 1 or 10. AD620ANZ is selected as the in-amp to do this measurement. Figure 1.5 and Figure 1.6 show the curves of DC offset over frequency from 100 kHz to 500 MHz with different forward RF power.

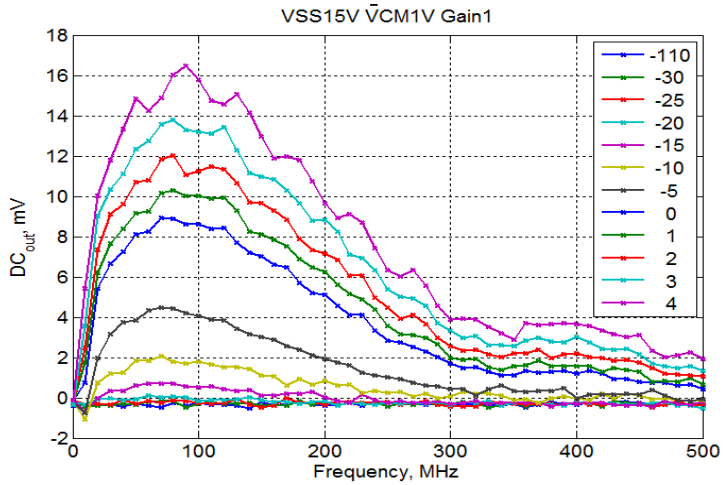

Figure 1.5. DC Offset over frequency when gain is 1

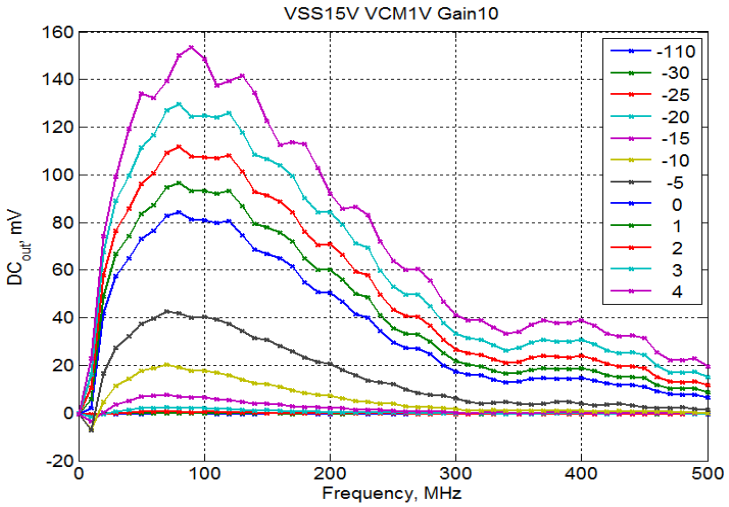

Figure 1.6. DC Offset over frequency when gain is 10

From the results, it can be observed that DC offset depends on the frequency and power level of injected RF noise, as well as the gain setting of AD620ANZ. The larger the power level of injected RF noise and gain setting of in-amp, the larger the DC offset.

1.3.2. Comparison Of Different IN-AMPS In Terms Of RF Noise Rectification. There are plenty of in-amps available in the market now. Comparison of their behavior in terms of RF noise rectification will help engineers select the right IC. In this thesis, the rectification behavior of popular instrumentation amplifiers is measured in both common mode and single-ended RF noise injection. Figure 1.7 shows the comparison of different ICs in common mode RF noise injection. Figure 1.8 shows the comparison of different ICs in single-ended RF noise injection. The forward RF noise level from RF generator is 0dBm in common mode RF noise injection and -16dBm in single-ended RF noise injection. In both cases, the gain of in-amps is set to 10.

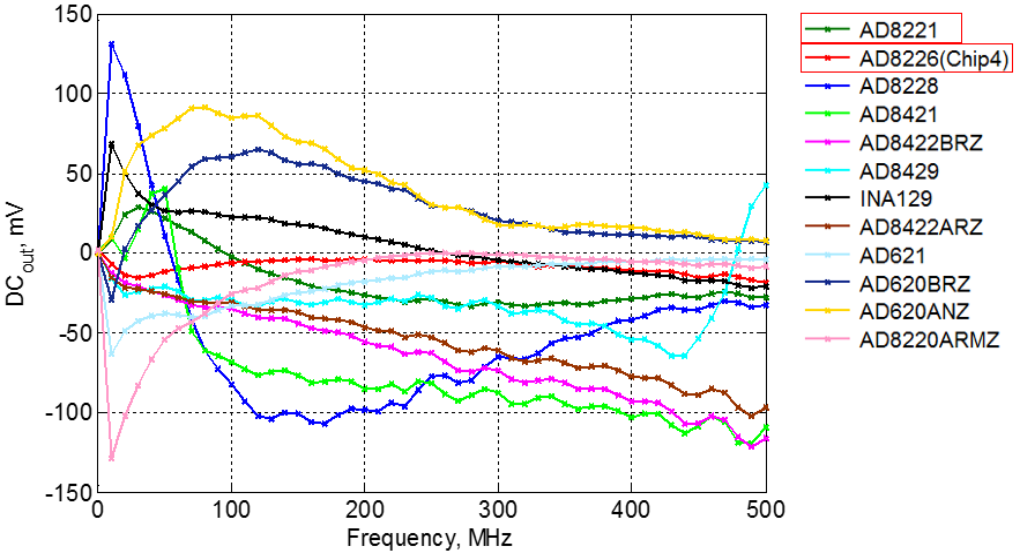

Figure 1.7. Common mode RF noise injection

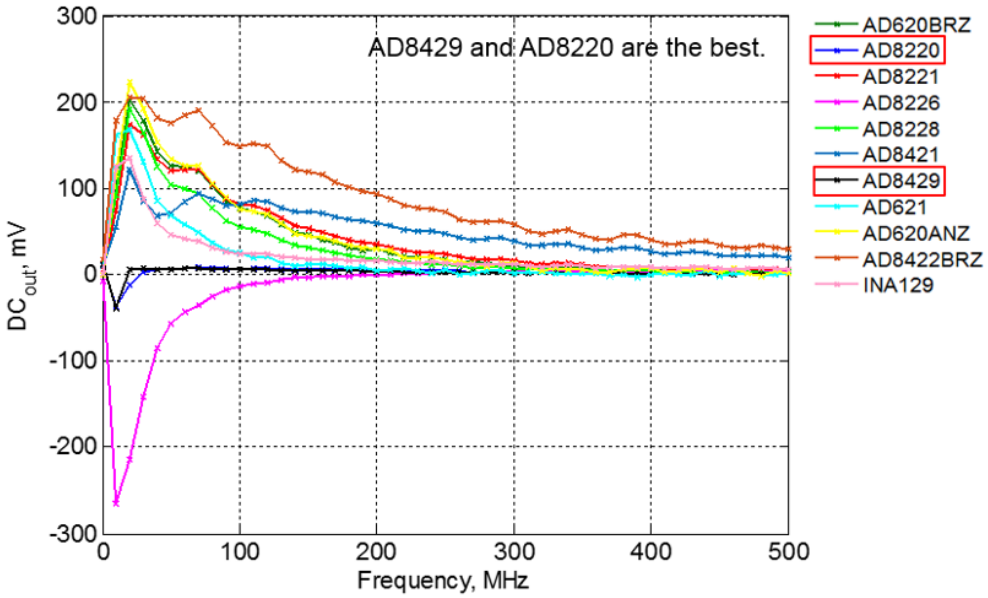

Figure 1.8. Single-ended RF noise injection

Though AD8226 shows least DC offset at output in common mode RF noise injection environment, different chips of AD8226 show large variations of DC offset at output with 0 dBm RF noise forwarded as shown in Figure 1.9. So AD8221 is recommended in common mode RF noise injection environment. And AD8220 and AD8429 are recommended in single-ended RF noise injection environment.

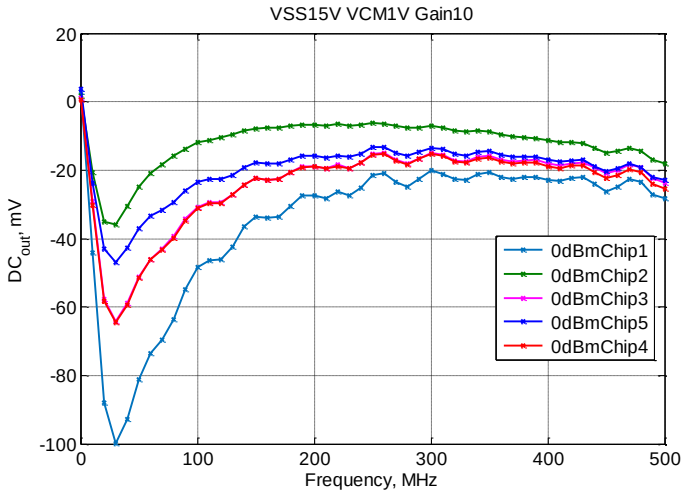

Figure 1.9. Comparison of different chips of AD8226

Also, it can be seen that single-ended RF noise injection shows larger DC offset than common mode RF noise injection with the same power level of injected RF noise, because in single-ended RF noise injection environment, when the power level of forward RF noise is -16 dBm, more or less the same DC offset show up in the output as common mode RF noise injection with 0 dBm RF noise forwarded. To further demonstrate this, AD620ANZ is taken as an example and the DC offset at output in common mode RF noise injection environment and single-ended RF noise injection environment both with 0dBm RF noise forwarded is compared. The result is shown in Figure 1.10.

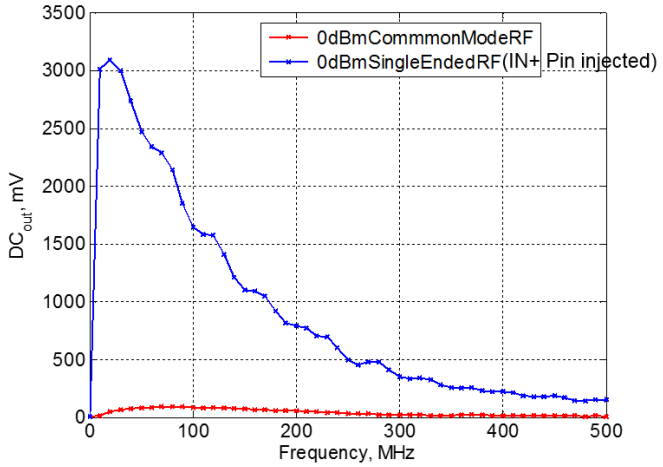

Figure 1.10. Comparison of single-ended RF noise injection and common mode RF noise injection

1.4. MECHANISM OF RF NOISE RECTIFICATION INSIDE IN-AMPS

It can be observed from Figure 1.5 and Figure 1.6 that the DC offset at output is basically proportional to the gain setting of AD620ANZ. This can be explained by the fact that rectification mainly happens at the non-inverting input of two op-amps in the first stage of an in-amp. The DC voltage difference between inverting input and non-inverting input of the in-amp is further amplified, which will cause a large DC offset at the output. Although there may still exist some out-of-band noise at the input of second stage, the RF noise there is usually much weaker and produces a negligible DC offset at the output. Therefore, in the case of Figure 1.5 and Figure 1.6, when the injected common mode RF noise is the same, DC voltage difference at the input of the in-amps will be the same and the DC output will be directly proportional to the gain setting. This can also explain why single-ended RF noise injection shows larger DC offset than common mode RF noise injection with the same power level of injected RF noise. Because in single-ended RF noise injection, DC voltage will be generated at only one input of the in-amp, which will produce a larger DC voltage difference between inverting input and non-inverting input of the in-amp.

In order to further verify above conclusion, an experiment is designed as follows. An in-amp is built from three op-amps (lm741) as shown in Figure 1.11.

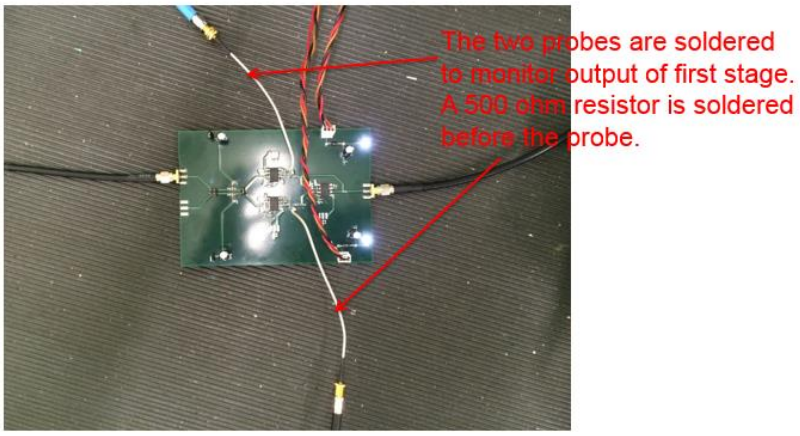

Figure 1.11. An in-amp built from three op-amps

Step1: Measure the DC output when RF noise is injected in the non-inverting pin of one op-amp in the first stage of self-built in-amp as shown in Figure 1.12. The op-amp is configured as a voltage follower. The DC output is named as V1.

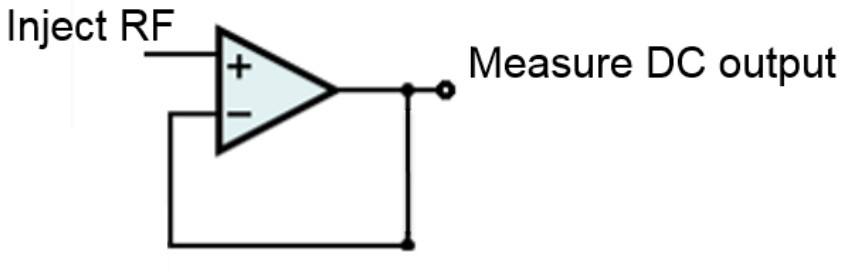

Figure 1.12. Characterization of op-amp in terms of RF noise rectification

Step2: Repeat step1 to characterize the other op-amp in the first stage of self-built in-amp. The DC output is named as V2.

Step3: Vout = (V2-V1)*Gain, and Gain is just the gain of the in-amp.

Step4: The calculated Vout in step3 is compared with direct measurement where common mode RF noise is injected into the in-amp.

Note that the injected RF noise level in step 1,2 and 4 should be the same. Since the op-amp is configured as a voltage follower, V1 and V2 are equal to the rectified DC voltage at non-inverting inputs of two op-amps, or inputs of the in-amp. The calculated Vout in step3 will be the amplified voltage of DC voltage difference. The calculated Vout in step3 matches well with direct measurement in step4 as shown in Figure 1.13, which verifies previous conclusion that rectification mainly happens at the non-inverting input of two op-amps in the first stage of an in-amp.

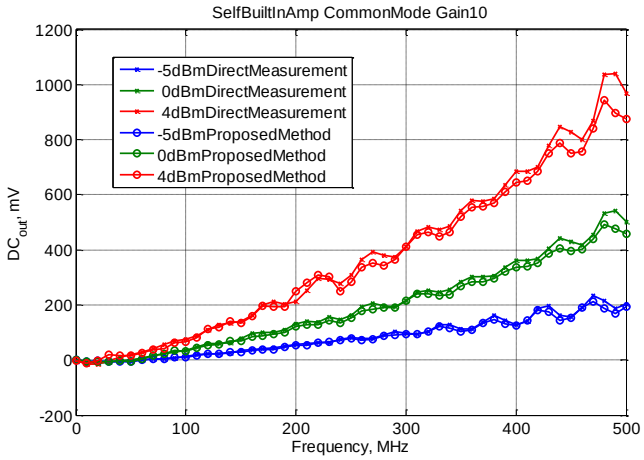

Figure 1.13. Comparison of direct measurement and calculated DC offset

1.5. WAYS TO REDUCE DC OFFSET AT THE OUTPUT

From previous analysis, it can be concluded that the main way to reduce DC offset at the output is to reduce the DC voltage difference generated by RF noise at the input of in-amps since gain is usually decided by actual use. As shown in Figure 1.10, it is always desirable if the RF noise is injected in common mode, which can reduce the DC voltage difference at the input. If the RF noise is already injected in common mode, a good way of reducing the DC offset is to make the first stage of in-amps as symmetric as possible so that the generated DC voltages at the inverting input and non-inverting input of in-amps are close and DC voltage difference is small. The asymmetry can come from difference of the two op-amps or the layout of the first stage.

For most in-amps in the market, the two op-amps of the first stage is already fixed but the gain resistor can be selected by the use to configure the desired gain. In the routing of the gain resistor, asymmetry can rise up. To show how sensitive RF noise rectification is to asymmetry of routing of gain resistor, rectification behaviors of AD620 when a 1pF SMT capacitor is added to one side of the gain resistor, a 1pF SMT capacitor is added to the other side of the gain resistor, two 1pF SMT capacitors are added to both sides of the gain resistor and no capacitor is added are compared. The compared result is shown in Figure 1.14.

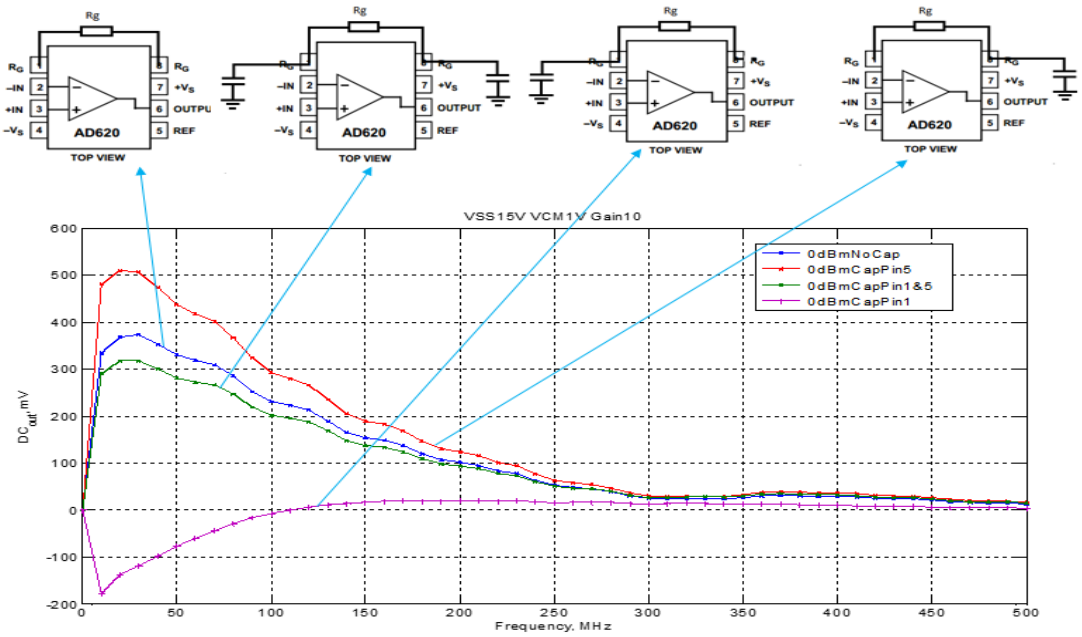

Figure 1.14. Symmetry test

If the 1pF capacitor is not added symmetrically, the RF rectification behavior will change dramatically. And Capacitances of an order of 1pF can easily arise from the parasitic effect of the traces.

To further verify this, RF rectification behavior of AD8221 with new layout (symmetric) and old layout (asymmetric) is compared. The result is shown in Figure 1.15. Asymmetric layout can cause DC offset at the output increase a lot.

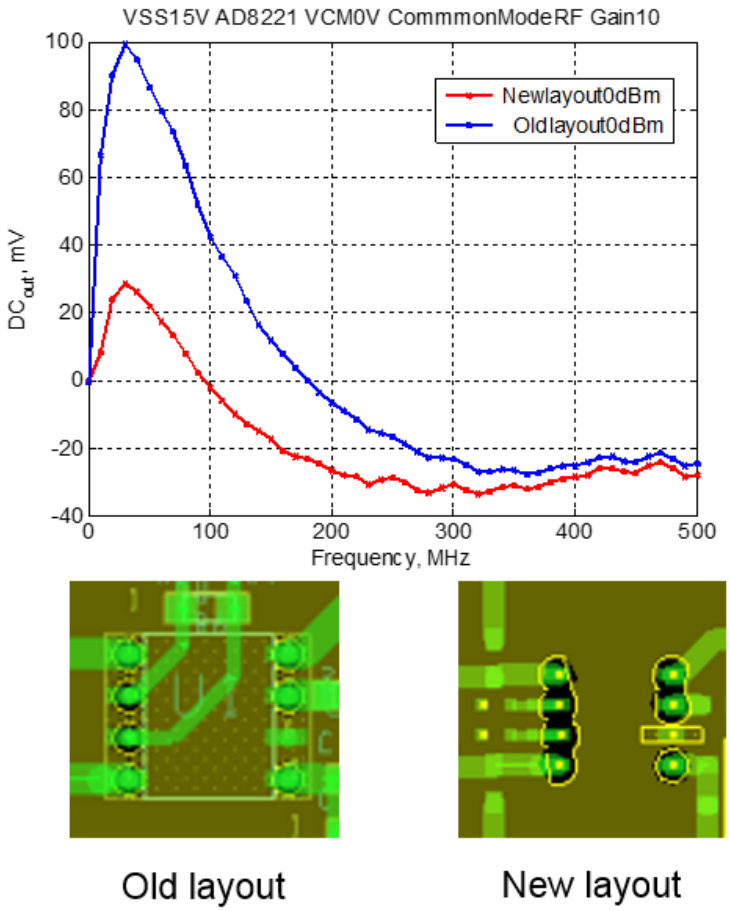

Figure 1.15. Effect of layout of gain resistor

1.6. CONCLUSION

In this thesis, the rectification behavior of popular instrumentation amplifiers is measured in both common mode and single-ended RF noise injection. It is recommended that AD8221 be used in common mode RF noise injection environment. And AD8220 and AD8429 are recommended in single-ended RF noise injection environment. The mechanism of RF noise rectification inside in-amps is also discussed. It is verified that rectification mainly happens at the non-inverting input of two op-amps in the first stage of an in-amp. The DC voltage difference between inverting input and non-inverting input of the in-amp is further amplified, which will cause a large DC offset at the output. It is shown that symmetry of the first stage in an instrumentation amplifier is very important.

The asymmetry of the first stage will increase the DC offset at the output dramatically. The layout of gain resistor should be symmetric to reduce DC offset at the output.

2. ESTIMATING THE NEAR FIELD COUPLING FROM SMPS CIRCUITS TO A NEARBY ANTENNA USING DIPOLE MOMENTS

2.1. INTRODUCTION

As wireless electronic products are becoming smaller and smaller while functions of these products are becoming more and more diverse, the density and complexity of electronic components inside are also increased. Radio frequency interference (RFI) through near field coupling from these electronic components to a nearby victim antenna is becoming one of the common issues in real products. Thus, a method of estimating the near field coupling in the pre-design process is desirable.

A lot of work to model the near field coupling has been done. In [4], an improved dipole-moment model as equivalent source to replace radiating source is investigated. The dipole-moment model is extracted based on near-field scanning. In [5] the near-field scanning size is studied. The dipole moments can be imported into full-wave simulation tool to simulate the near field coupling, as illustrated in [6]. However, the method is only validated by simulation and the scenario is quite simple in [6]. A decomposition method based on reciprocity to estimate the near field coupling from radiating source to victim antenna is presented in [7]. And this method is validated by measurement in [8], where the near field coupling from an IC to a victim antenna is studied.

Switched Mode Power Supplies (SMPS) are commonly used in modern electronic systems due to their high power conversion efficiency, smaller size and lighter weight. However, their switching currents, if not carefully suppressed, can cause RFI problems through near field coupling or conduction by power traces. In [9], the conducted emissions are modeled using total voltage method.

In this thesis, the near field coupling from SMPS circuits to a nearby antenna is studied using dipole moments. The dipole moments are extracted from scanned H fields on a plane above SMPS circuits, and then imported into an HFSS model to do full wave simulation.

To investigate the near field coupling from SMPS circuits to a nearby victim antenna, a test board is designed and manufactured as shown in Figure 2.1. Decoupling capacitor and ferrite beads are added in the DC power supply path to prevent possible radiation from the power cable. The antenna resonates at around 880MHz.

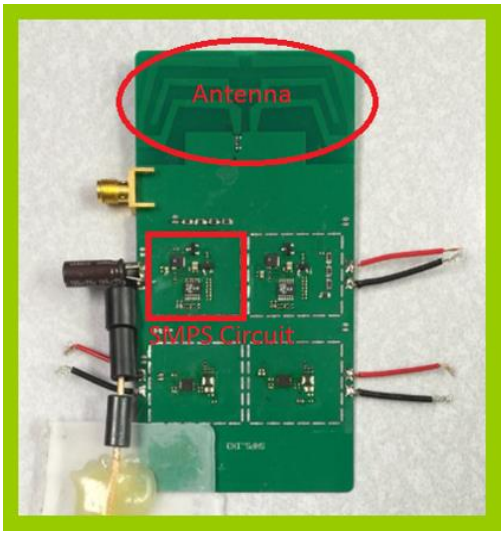

Figure 2.1. The test board

The near field coupling measurement using spectrum analyzer with different RBW settings is shown in Figure 2.2. From the measurement result, it's shown that the coupled noise is a broad band signal since the noise level increases with RBW. This comes from the randomness of time domain waveform of SMPS noise, which results in a fixed power spectral density in the frequency domain.

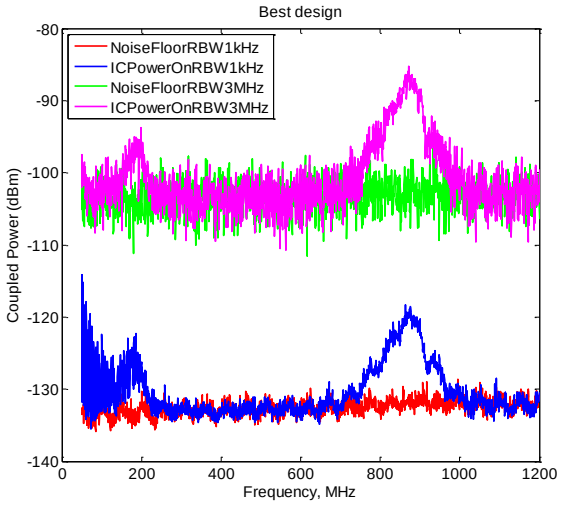

Figure 2.2. Measured coupling from SMPS circuits to antenna with different RBW setting

2.2. NEAR FIELD SCAN

2.2.1. How To Resolve Phase. To resolve the phase of near field of SMPS noise, two methods can be used. The first method is to use oscilloscope to capture the time domain waveform of near field signal and reference signal as shown in Figure 2.3 and then apply FFT to both time domain waveform to get the frequency domain components of two signal. The near field probe is used to convert time-changing H fields into measurable voltage [10]. The reference signal is taken from the SMPS circuits.

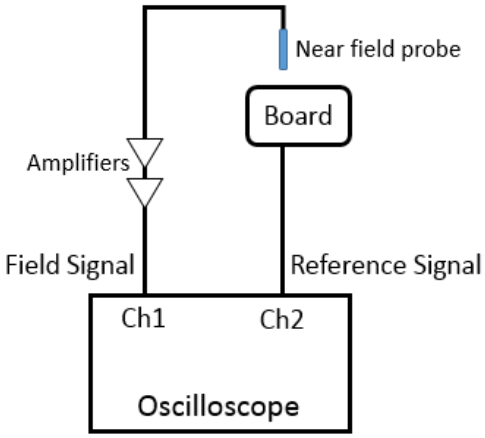

Figure 2.3. Measurement setup to resolve phase using oscilloscope

The relative phase of near field is calculated as:

Relative Phase = Phase of Field Signal – Phase of Reference Signal

The time domain waveform of field signal and reference signal is shown in Figure 2.4. In each period, there are two pulses which are directly related with the switch-on and switch-off of SMPS circuits.

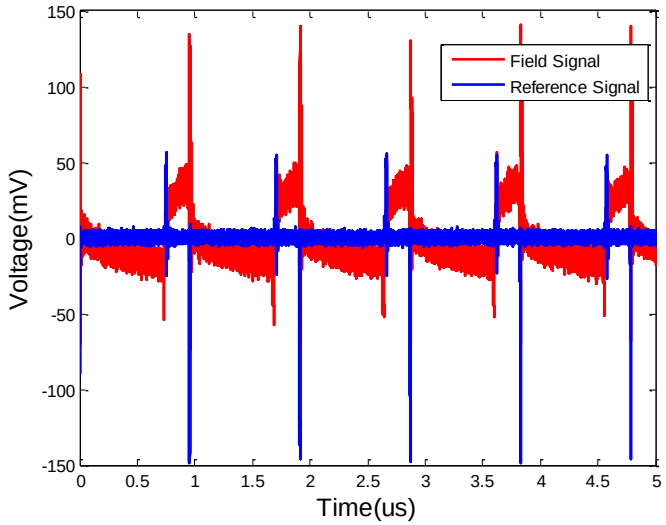

Figure 2.4. Time domain waveform of field signal and reference signal

As shown in Figure 2.5, the falling edge (-80mV) of reference signal is triggered and time domain waveform of field signal and reference signal is put in one period. The waveform is zoomed in to show the first pulse and the second pulse. It's seen that time domain waveform of field signal and reference signal has both random noise and jitter. This jitter comes from the variation of duration between pulses.

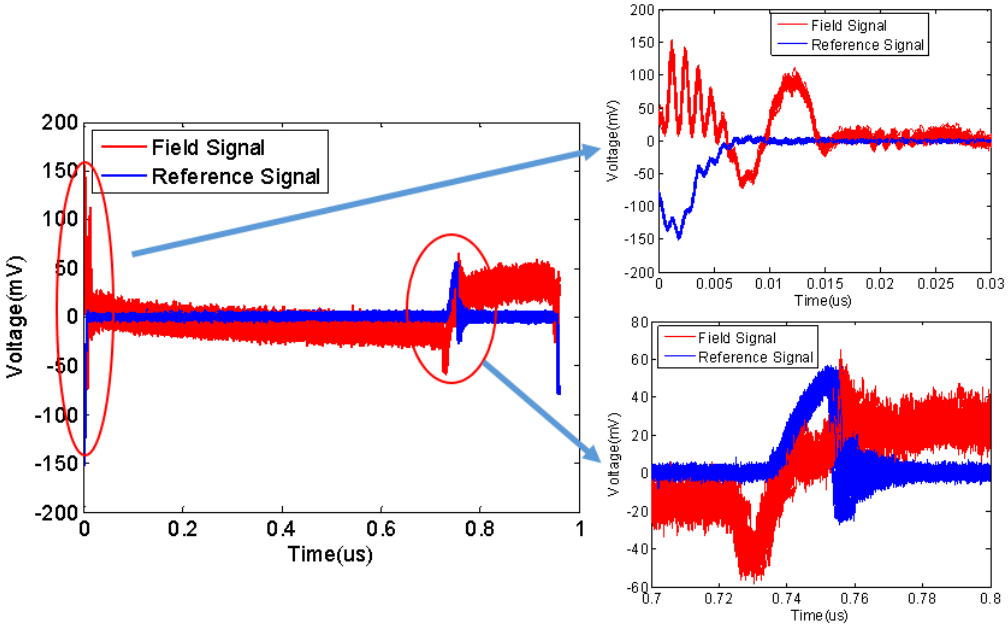

Figure 2.5. Time domain waveform in one period

To remove the random noise in the time domain, average must be activated. Since jitter exists, the waveform of pulses, except the first one which is aligned by triggering, will be distorted once average is activated. For this reason, only one period is captured during the scan. Although the second pulse is also distorted in one period, its pulse width is larger than the total jitter and the waveform will not change much. In addition, it does not contain as much high frequency components as the first one and will not contribute much to the high frequency coupling. The captured waveform during scan after averaging is shown in Figure 2.6. Then FFT is applied to captured waveform and relative phase is calculated using formula (1).

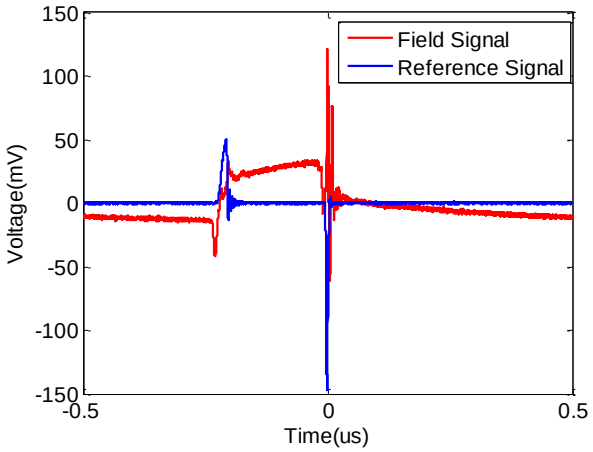

Figure 2.6. Captured waveform during scan

The second method is to use VNA tuned receiver mode, as illustrated in [11]. The scanning setup is shown in Figure 2.7. The field signal and reference signal are fed into two receivers of VNA, and the angle of A/B is taken as the phase. Average is activated to increase the accuracy of phase measurement. Both reference signal and probe signal need to be above the noise floor of receivers in the desired frequency, so amplifiers are added in both signal channels.

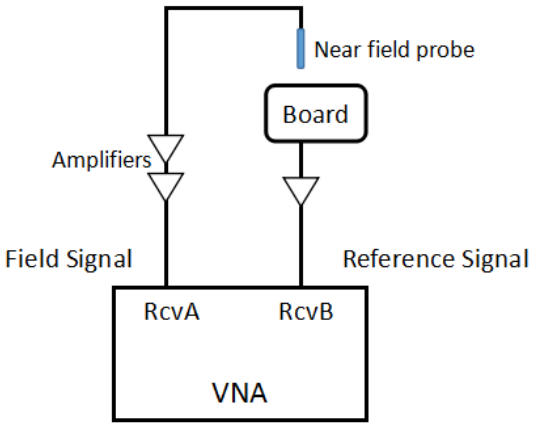

Figure 2.7. Measurement setup to resolve phase using VNA

The scanned phase pattern of H field in x direction at 870MHz using both methods is shown in Figure 2.8.

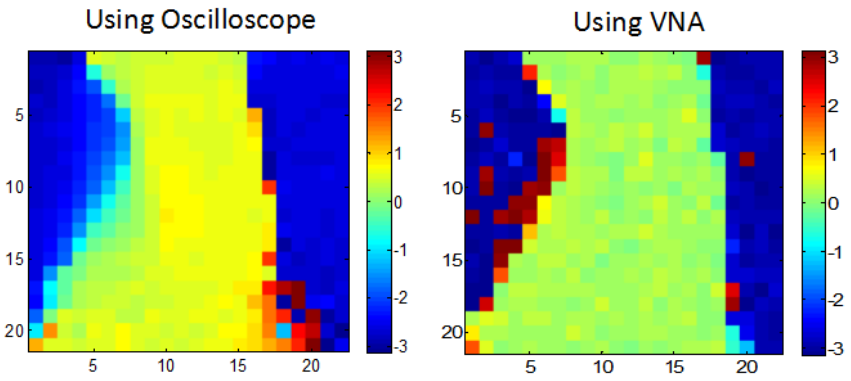

Figure 2.8. Scanned phase pattern of H field in x direction at 870MHz

2.2.2. How To Resolve Magnitude. As shown in Figure 2.2, the SMPS noise is a broad band noise which has a fixed power spectral density. To acquire the equivalent magnitude at certain frequency with corresponding RBW setting, spectral density estimation (SDE) needs to be done [12]. Direct FFT is not meaningful for this random signal. Another simple yet effective method is to using spectrum analyzer with same RBW setting as the coupling measurement to do one more scan to resolve magnitude. The scanning setup and scanned magnitude pattern of H field at 870MHz with a RBW setting of 1 kHz is shown in Figure 2.9. The unit is dB A/m.

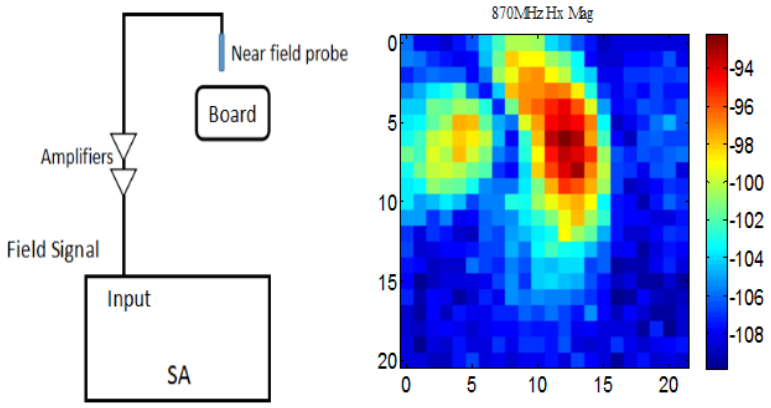

Figure 2.9. Scanning setup for magnitude and
scanned magnitude pattern of H field in x direction at 870MHz

2.3. DIPOLE-MOMENT MODEL EXTRACTION AND USAGE

Based on [4], an improved dipole moment model can be used to represent the radiation source. In this model, an array of vertical Hertzian electric dipole moment P_z and horizontal magnetic dipole moments M_x and M_y with uniform space are chosen to represent the radiation source. The values of these dipole moments are determined from the near field measurements in a scanning plane above the radiation source as shown in Figure 2.10. An infinitely large ground plane is assumed and image dipoles are introduced so that effects of the ground plane is not included in the dipole moments. The multiple scattering inside the radiation source is neglected otherwise the case will be too complex.

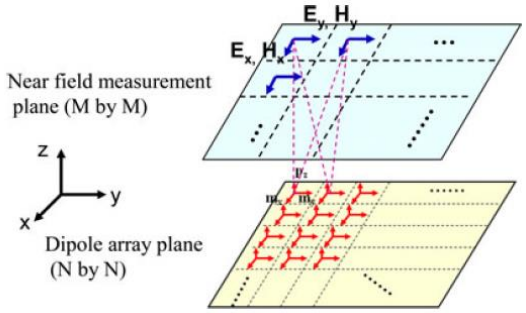

Figure 2.10. Near field scan plane and dipole array plane[4]

Assuming the size of near field plane is M by M and the size of dipole array plane is N by N(they can have any size, but it will affect the accuracy of extracted dipole moments), the fields generated by the array of all three kinds of dipole moments can be formulated by (2).

$$\begin{bmatrix} [H_x]_{M^2\times 1} \\ [H_y]_{M^2\times 1} \end{bmatrix} = T \begin{bmatrix} [P_z]_{N^2\times 1} \\ [M_x]_{N^2\times 1} \\ [M_y]_{N^2\times 1} \end{bmatrix} \qquad (2)$$

where the T matrix can be expressed by (3).

$$T = \begin{bmatrix} T_{H_xP_z} & T_{H_xM_x} & T_{H_xM_y} \\ T_{H_yP_z} & T_{H_yM_x} & T_{H_yM_y} \end{bmatrix} \qquad (3)$$

T matrix is the transfer function relating horizontal H field on the scanning array plane to a certain dipole moment on the dipole array plane [13]. For eaxample, T_{HxPz} represents H fields in the x direction generated by Pz dipoles. Each submatrix has a size of M^2 by N^2. The ground's effect must be considered in the T matrix. Equation (2) can be rewritten as (4) after normalization is applied to both field vector and dipole moments vector.

$$F_n = T_{nk} X_k \qquad (4)$$

The horizontal H fields on the scanning array plane are already known from near field scan, so F_n is known. The transfer function T_{nk} is known as well, then least square method is used to solve X_k. Dipole moment array can be obtained from X_k.

Dipole moments as source is supported in HFSS. An example text file describing the dipole information is shown in Figure 2.11. With this text file, it's possible to incorporate a large number of dipole moments into a HFSS model. The HFSS model with all the extracted dipole moments imported is shown in Figure 2.12.

```
$begin 'IncHDWave1'
        ID=37
        BoundType='Hertzian-Dipole Incident Wave'
        ParentBndID=-1
        IsCartesian=true
        EoX='0'
        EoY='0'
        EoZ='1'
        kX='0'
        kY='0'
        kZ='1'
        PhiStart='0deg'
        PhiStop='0deg'
        PhiPoints=1
        ThetaStart='0deg'
        ThetaStop='0deg'
        ThetaPoints=1
        EoPhi='1'
        EoTheta='0'
        OriginX='0.0017meter'
        OriginY='0.0635meter'
        OriginZ='0.0027115meter'
        SphereRadius='0.001meter'
        IsElectricDipole=true
$end 'IncHDWave1'
```

Position of dipole

Electric or magnetic?

Figure 2.11. An example text file describing the dipole information in HFSS

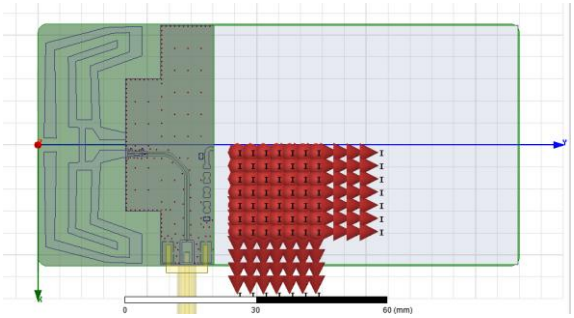

Figure 2.12. HFSS model with dipole moments imported

2.4. COMPARISON OF SIMULATION AND DIRECT MEASUREMENT

After the dipole moments are imported into HFSS model, the near field coupling can be simulated through full wave simulation. A comparison of simulation and direct measurement is shown in Figure 2.13 and Table 2.1. The simulated result matches well with direct measurement and the largest error is 4.9 dB.

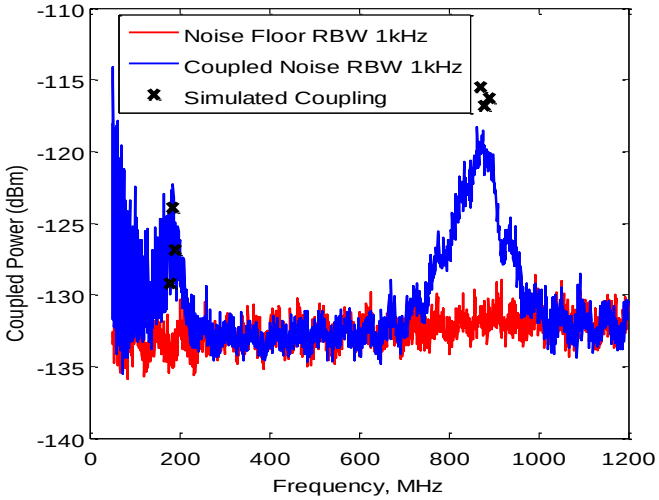

Figure 2.13. Comparison of simulation and direct measurement

Frequency(MHz)	Simulation(dBm)	Measurements(dBm)
180	-129.2	-130.0
185	-123.9	-124.7
190	-126.9	-126.0
870	-115.5	-119.9
880	-116.8	-121.6
890	-116.3	-121.2

Table 2.1. Comparison of simulation and direct measurement

2.5. CONCLUSION AND ERROR ANALYSIS

This thesis presents a method to estimate near field coupling from SMPS circuits to a nearby antenna. Although validated by this specific example, it can be applied to other RFI scenario as well.

There are two key factors in this method. The first factor is that the dipole moments should represent source well. This requires that near field scan be correctly done and dipole extraction parameters like number of dipoles, dipole position and so on

be appropriately chosen. Before importing the extracted dipole moments into HFSS model to do full wave simulation, validation of the correctness of extracted dipole moments needs to be done. One common method is to scan another plane above the source and compare the scanned H field with calculated one using extracted dipole moments. A good match shows that dipole moments can represent source well. The other one is that the simulation model should be accurate. An accurate model is not always available. And the difference between model and real product is one of the common error sources. As shown in Figure 2.13, the error is larger at around 880MHz. The reason behind this is that the antenna model is not accurate at its resonant frequency, as shown in Figure 2.14.

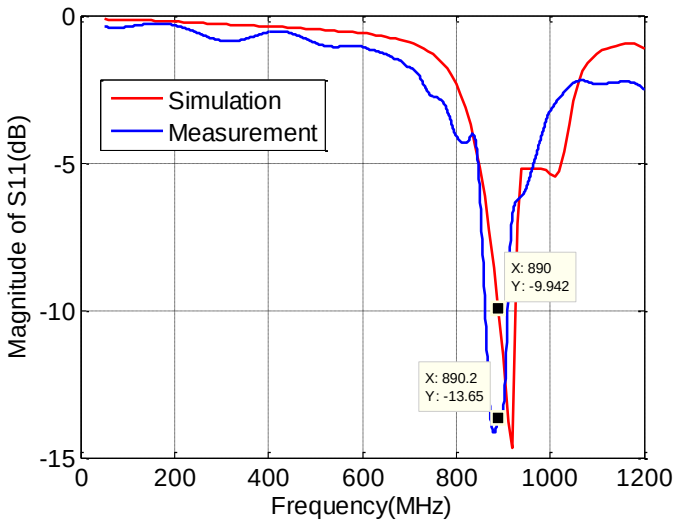

Figure 2.14. S11 of antenna in simulation model and measurement

BIBLIOGRAPHY

[1] R.F. Coughlin, F.F. Driscoll Operational Amplifiers and Linear Integrated Circuits (2nd Ed.1982. ISBN 0-13-637785-8) p.161.

[2] Moore, Davis, Coplan Building Scientific Apparatus (2nd Ed. 1989 ISBN 0-201-13189-7)p.407.

[3] Hall, Chris. "EMI Rejection Ratio of Operational Amplifiers (With OPA333 and OPA333-Q1 as an Example)." (2011).

[4] Yu, Zhenwei, et al. "An improved dipole-moment model based on near-field scanning for characterizing near-field coupling and far-field radiation from an IC." Electromagnetic Compatibility, IEEE Transactions on 55.1 (2013): 97-108.

[5] X. Ren et al., "The impact of near-field scanning size on the accuracy of far-field estimation," 2014 IEEE International Symposium on Electromagnetic Compatibility (EMC), Raleigh, NC, 2014.

[6] Pan, Jingnan, et al. "Application of dipole-moment model in EMI estimation." Electromagnetic Compatibility (EMC), 2015 IEEE International Symposium on. IEEE, 2015.

[7] Wang, Hanfeng, et al. "Estimating radio-frequency interference to an antenna due to near-field coupling using decomposition method based on reciprocity." Electromagnetic Compatibility, IEEE Transactions on 55.6 (2013): 1125-1131.

[8] Li, Liang, et al. "Measurement validation for radio-frequency interference estimation by reciprocity theorem." Electromagnetic Compatibility (EMC), 2015 IEEE International Symposium on. IEEE, 2015.

[9] Wang, Yansheng, et al. "Conducted-emission modeling for a switched-mode power supply (SMPS)." Electromagnetic Compatibility and Signal Integrity, 2015 IEEE Symposium on. IEEE, 2015.

[10] Chuang, Hao-Hsiang, et al. "A magnetic-field resonant probe with enhanced sensitivity for RF interference applications." Electromagnetic Compatibility, IEEE Transactions on 55.6 (2013): 991-998.

[11] Li, Tianqi. Radio Frequency Interference (RFI) Modeling of Complex Modules in Mobile Devices and System-level Modeling for Transient ESD Simulation. MISSOURI UNIVERSITY OF SCIENCE AND TECHNOLOGY, 2014.

[12] Stoica, Petre, and Randolph L. Moses. Introduction to spectral analysis. Vol. 1. Upper Saddle River: Prentice hall, 1997.

[13] Balanis, Constantine A. Antenna theory: analysis and design. Vol. 1. John Wiley & Sons, 2005.

VITA

Chunyu Wu was born in Chibi, Hubei, China. He received his bachelor's degree in Electronic Information Engineering in Huazhong University of Science and Technology in 2014. He enrolled in ECE department of Missouri University of Science and Technology in August, 2014. Since then, he worked as a graduate research assistant in Electromagnetic Compatibility Laboratory. His main research interest includes signal integrity, electromagnetic compatibility and radio frequency interference. He received his Master's Degree in Electrical Engineering in May 2017.